

# Fast multiscale kinetic Monte Carlo simulations of three-dimensional self-assembled quantum dot islands

R. Zhu,<sup>1</sup> E. Pan,<sup>1,\*</sup> and P. W. Chung<sup>2</sup>

<sup>1</sup>*Department of Civil Engineering and Department of Applied Mathematics, University of Akron, Akron, Ohio 44325, USA*

<sup>2</sup>*U.S. Army Research Laboratory, Aberdeen Proving Ground, Maryland 21005, USA*

(Received 25 November 2006; revised manuscript received 18 January 2007; published 25 May 2007)

A three-dimensional kinetic Monte Carlo model is developed to simulate the growth of self-assembled quantum dot islands. Our multiscale model includes the long-range strain energy contribution from a fast continuum Green's function calculation and an up-down ratio describing the relative probability for atoms to jump out of the plane of the surface during the growth process. For the model material InAs/GaAs(001), we studied the effect of the flux rate and the deposition and interruption times on the island shape and ordering, which shows that a lower flux rate and a longer growth time correspond to a better island distribution. We also successfully simulated the relation between the island height and the up-down ratio. It is observed that for an up-down ratio between 1 and 20, the island height increases dramatically with increasing up-down ratio, reaching an inflection point around 13. When the up-down ratio continues to increase from 20, the island height approaches a constant value at about 20 grids. The critical up-down ratio 13 signifies the transition from a flat cluster growth mode to a sharp three-dimensional island growth mode.

DOI: [10.1103/PhysRevB.75.205339](https://doi.org/10.1103/PhysRevB.75.205339)

PACS number(s): 68.65.Hb, 68.03.Hj, 68.55.Ac, 68.43.Jk

## I. INTRODUCTION

Self-assembled quantum dots (QDs) are intensively studied due to their unique optical and electronic properties, with potential applications in optoelectronics and semiconductor devices.<sup>1,2</sup> The InAs/GaAs heterostructure is a typical example; it is characterized by a large lattice mismatch and undergoes a growth transition from a two-dimensional (2D) layer to three-dimensional (3D) islands.<sup>3,4</sup> The optical properties in the 2D layer and 3D islands have also been studied.<sup>5</sup>

Experimental data indicate that synthesis of an InAs/GaAs island array is sensitive to ambient growth parameters, exhibiting both thermodynamic and kinetic features.<sup>6,7</sup> The mechanisms behind the transition from flat pyramids to sharp domes have been studied intensively.<sup>8-13</sup> Using atomic force microscopy, Arciprete *et al.*<sup>13</sup> showed clearly that different coverage usually corresponds to different QD size. The transition from thermodynamically to kinetically controlled QD self-assembly was also studied by Musikhin *et al.*,<sup>14</sup> both experimentally and theoretically.

It is argued that surface diffusivity and mobility could be affected by the strain field on the surface and even by the quantum size effect.<sup>15-19</sup> Recent first-principles calculations of Si and Ge adatoms on Si(001) and Ge(001) surfaces showed clearly the correlation between the surface diffusion and mobility and the applied strain field.<sup>15</sup> Diffusion anisotropy of adatoms due to the applied strain field was also observed,<sup>15</sup> and enhanced evaporation caused by the local strain was further reported.<sup>20</sup> The epitaxial system can maintain a lower free energy by transferring atoms from the island edge to the upper layer, because the transition leads to a decrease in the contact area between the substrate and a new layer.<sup>13</sup> Thus, atomic transitions to the upper layers lead to a relaxation in the local strain field. The tradeoff between the cost of the additional surface energy and the gain of energy due to elastic relaxation is the very driving force for the transition from flat pyramids to sharp domes.<sup>11,12,18,19,21,22</sup>

These arguments provide reason enough to consider situations where the atom hopping probability to an upper layer can be higher than that to a lower layer. The kinetics of such a process could be described by adjusting the probability for atoms to hop up or hop down, which could subsequently lead to flat cluster or sharp 3D island self-assembly, and ultimate control over synthesis mechanisms.

While some simple computational approaches for QD self-assembly have been discussed before (e.g., Ref. 23), no complete 3D QD self-assembly model has been developed so far in which the growth from flat cluster to 3D islands and the corresponding island size equalization can be clearly illustrated during the growth process. Such a model would be vital to understanding the parametric variations of surface patterns to conventional growth parameters such as flux rate, interruption time, and temperature, among others. We therefore propose a fast multiscale 3D kinetic Monte Carlo (KMC) QD growth model. It is developed from our original  $(x,y)$ -plane growth model<sup>24,25</sup> by a fast algorithm for the long-range strain energy calculation and by introducing the up-down ratio for lateral self-organization. We remark that, while the material parameters in our simulation are for InAs/GaAs(001), the two species (In and As) in the InAs QD islands are assumed to be equal. In other words, they are indistinguishable in the KMC simulation.<sup>25</sup>

With the proposed program, we have successfully simulated the transition of QD flat clusters to 3D islands in the model InAs/GaAs(001) system, with results consistent with the experimental observations and numerical simulations based on different approaches.<sup>8,12,18</sup> Furthermore, depositions with different flux rates are studied to show how the flux rate affects the island equalization during the deposition process. Our model has also shown clearly the importance of the interruption time during the growth of QD islands. We believe that this model will provide an attractive means for simulating strain-controlled ordering of QDs on surfaces.

## II. MODEL DESCRIPTION

The 3D layer-by-layer KMC growth model is developed from our 2D  $(x,y)$ -plane growth model<sup>24,25</sup> where diffusion of the InAs compound (on the surface of GaAs substrate) was simulated by assuming them as a single species with cubic crystal structures [see, e.g., Ref. 26]. As in our previous model, the important contribution from the long-range elastic strain energy is included using a fast algorithm based on the Green's function method.<sup>27,28</sup> Furthermore, to account for the adsorption and desorption motion of the atoms,<sup>29,30</sup> an up-down ratio is introduced.<sup>23</sup>

First, the 2D hopping probability of an atom from one lattice site to a nearest or next nearest neighbor site in the  $(x,y)$  plane is still governed by the Arrhenius law, enhanced by the long-range strain energy field and an additional Schwöbel step-edge barrier for monatomic step crossing.<sup>24–26,31–34</sup> The hopping probability is given by

$$p = \nu_0 \exp\left(-\frac{E_s + E_n - E_{\text{str}}(x,y)}{k_B T}\right), \quad (1)$$

where  $\nu_0$  is the attempt frequency ( $=10^{13} \text{ s}^{-1}$ ),  $T$  the temperature, and  $k_B$  the Boltzmann constant. Also, in Eq. (1),  $E_s$  and  $E_n$  are the binding energies to the surface and to the neighboring atoms, respectively. Finally,  $E_{\text{str}}(x,y)$ , a function of the plane coordinates  $(x,y)$ , is the energy correction from the long-range strain field due to the lattice misfit between the substrate and the deposited material. We remark that, while the importance of strain for diffusion was addressed via first-principles calculation<sup>15</sup> assuming a uniform axial or biaxial strain field, with some interesting results for the strain-induced diffusion and mobility features, the strain field and the corresponding strain energy are calculated in this paper using the Eshelby inclusion theory combined with the Green's function solution.<sup>27,28</sup> The required input parameters are the bulk elastic stiffness tensor and lattice misfit of InAs/GaAs(001). The specific chemical species selected for these simulations are implied in the definition of the strain energy. Furthermore, as this long-range strain energy needs to be calculated repeatedly during the simulation, we have developed a fast algorithm by precalculating the strain energy along a unit circle and then interpolating its value at any location afterwards.<sup>27,28</sup>

We calculate the binding energy to the neighboring atoms in the  $(x,y)$  plane,  $E_n$ , using the following approach. We take the strength of all single nearest neighbor bonds  $E_b$  to be 0.3 eV, and reduce it by a factor of  $\alpha$  ( $=1/\sqrt{2}$ ) for the next nearest neighbors.<sup>34</sup> To evaluate the diffusion barrier, the binding energy at the site  $P_0$ , where the diffusing atom is located [one of the eight locations surrounding the center atom shown by the solid box in Fig. 1(b)], is calculated to be

$$E_{P_0} = nE_b + \alpha mE_b \quad (2)$$

with  $n \leq 4$  and  $m \leq 4$  being, respectively, the number of nearest and next nearest atoms. Similarly, for the site  $P_1$  to which the atom is going to hop [one of the 16 locations surrounding the solid box shown by the dashed box in Fig. 1(b)], we have

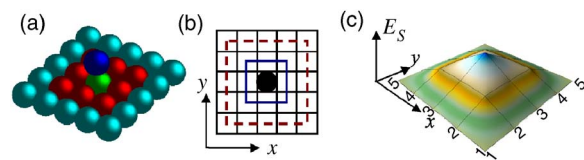


FIG. 1. (Color online) Schematic illustration of 3D QD self-assembly (cubic crystal) model. (a) An atom on top of the substrate surface  $(x,y)$  plane, (b) the relative locations of the atom grid on the  $(x,y)$  plane, and (c) the corresponding binding energy  $E_s$  related to the in-plane locations.

$$E_{P_1} = g(n'E_b + \alpha m'E_b) \quad (3)$$

where  $n' \leq 4$  and  $m' \leq 4$  are, respectively, the number of nearest and next nearest atoms at the new site  $P_1$ , and  $g$  describes the coupling between the adjacent lattice sites.<sup>34</sup> We point out that, while a small  $g$  corresponds to a weak coupling, a large  $g$  corresponds to a strong coupling. Following previous studies, we assume a weak coupling between the adjacent lattice sites with  $g=0.2$  in this paper.<sup>34</sup> Therefore, the overall binding energy  $E_n$  caused by neighbor interactions for an atom to jump from site  $P_0$  to site  $P_1$  is given by the difference of the binding energies at the corresponding lattice sites,

$$E_n = (n - gn')E_b + (m - gm')\alpha E_b. \quad (4)$$

Second, the binding energy to the surface of the  $(x,y)$  plane, i.e.,  $E_s$ , was assumed to be constant (actually,  $E_s = 1.3 \text{ eV}$ ) in our previous 2D  $(x,y)$ -plane self-assembly model.<sup>24,25</sup> In other words, in our 2D model, the atom diffusion on the surface was mainly controlled by the neighboring binding energy among the atoms on the surface as described by Eq. (4). It is apparent, however, that the relative position of the adatom with respect to the surface structure should influence the diffusion activity on the surface. Therefore, the surface binding energy should depend on the surface geometry of both the initial and final positions of the atoms. Based on recent molecular dynamics calculations<sup>35</sup> and KMC simulations<sup>24–26,34</sup> in 2D, we therefore propose the following simple equation for the 3D surface binding energy (Fig. 1):

$$E_s = (1 - g)E_{s,0} + (p - gp')\alpha E_{s,0} + (q - gq')\alpha\alpha E_{s,0}, \quad (5)$$

where  $E_{s,0}$  is the binding energy for the atom exactly under the selected adatom (Fig. 1),  $p, q$  are the numbers of nearest and next nearest atoms in the original position ( $p \leq 4, q \leq 4$ ),  $p', q'$  are the number of nearest and next nearest atoms in the new position ( $p' \leq 4, q' \leq 4$ ). The other two parameters  $g$  and  $\alpha$ , as in 2D, are used to scale the energy contribution from the atoms in the first and second squares [Fig. 1(a) and 1(b)]. Assuming that the maximum surface binding energy is 1.3 eV as before for the 2D growth simulation,<sup>24,25</sup> which means that all the positions under this adatom are occupied by atoms, we can find  $E_{s,0} = 0.28 \text{ eV}$  from Eq. (5) by back calculation.

Finally, as discussed in the Introduction, the growth system always tries to decrease its free energy by moving atoms at the edge to upper layers to form 3D islands. The probability for an atom to hop to an upper or lower layer depends on

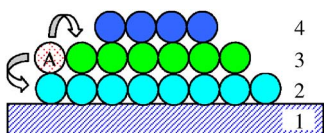


FIG. 2. (Color online) Illustration of the up or down jump for an edge atom  $A$  during 3D QD self-assembly.

the material properties and growth conditions,<sup>5,13</sup> and is assumed here to be the dominant mechanism that enables formation of out-of-plane structures during growth. To account for the up and down motion of the atoms, an additional parameter  $\rho$  is introduced,<sup>23</sup> which is defined as the ratio of the probability for edge atoms to hop up to that for hopping down. In other words, if we let  $P_{\text{up}}$  and  $P_{\text{down}}$  be the up and down probabilities, respectively, then the up-down ratio  $\rho = P_{\text{up}}/P_{\text{down}}$ . It is further remarked that the up-down ratio actually reflects the balance between surface energy increase and strain energy decrease.<sup>12,18</sup> This physical activity is illustrated in Fig. 2 where layer 1 is the substrate and the atom  $A$  is on the edge of layer 2 of the deposited atoms (i.e., within the QD island). It is also understandable that the up or down jump probability of atom  $A$  is controlled only by the up-down ratio instead of by the individual up and down jump probabilities. Moreover, strictly speaking, since the strain energy changes along the island height direction,<sup>36</sup> the up-down ratio will, in general, not be constant in different island layers (e.g., Ref. 37). However, in order to extract the important contribution of the up-down ratio, we assume that the up-down ratio  $\rho$  is constant and is affected only by the geometry around it but not by the layer position relative to the surface. Furthermore, in order to form 3D islands, the number of atoms jumping up should be larger than those jumping down, which means that the up-down ratio  $\rho$  should be larger than 1. Otherwise, all the atoms will tend to move to lower layers to form the atomically thin layer-by-layer Frank-van der Merwe structure.

The new 3D KMC simulation routine is similar to the 2D model we developed before,<sup>24,25</sup> but is extended to 3D with the jump ratio and enhanced by the fast strain energy calculation. In the program, atom diffusion processes are simulated one by one. Within the surface plane, each atom at most has four possible nearest and four possible next nearest diffusion positions [Fig. 1(b)], or four nearest (along the  $x$  and  $y$  directions) and four next nearest neighbors (along the two diagonal directions). Every possible diffusion step of a given atom is obtained by evaluating the probability  $p$  from Eq. (1), along with a given multiple-factor ( $P_{\text{up}}$  and  $P_{\text{down}}$ ) ratio for the probability of jumping up or down. These probabilities are stored and added to get the total diffusion probability for the atom. The total probability is then obtained by adding all the probabilities for the atoms together. During the simulation, an atom is randomly chosen to move to a new lattice site in accordance with its likelihood and the move is executed with those near the island edge subject to the Schwöbel barrier. The corresponding time interval  $\Delta t$  (i.e., proportional inversely to the overall probability) is calculated and added to the elapsed simulation time.<sup>26,34,38,39</sup> Since the movement of an atom also alters the diffusion barriers for the

neighboring atoms in the previous neighborhood as well as in the new one, the moving atom and all the atoms in its surrounding area have to be recalculated to obtain the new diffusion probabilities.

The strain energy is calculated based on the Green's function method<sup>27,28,40</sup> combined with a unique fast algorithm. First, it can be shown that, on the surface of an anisotropic semiconductor substrate, the strain energy due to a concentrated lattice misfit (source) is proportional to  $E(\theta)/r^6$ ,<sup>27,28,40</sup> where  $r$  and  $\theta$  are the in-plane polar coordinates with origin at the source point. Since the strain energy scales as  $1/r^6$ , one needs only to calculate the energy value along the circumference of the unit circle, i.e., one only needs  $E(\theta)$  using the Green's function solution; for the strain energy at any surface location  $r$  and  $\theta$ , the result is simply  $E(\theta)/r^6$ . Second, even though one can significantly reduce the execution time for the strain energy calculation using this precalculation approach, simulation of the strain energy at each jump step is still computationally very expensive. Fortunately, the strain energy changes only slightly with the motion of a single atom, and it is optimal to calculate the strain field at every 2000–3000 jump steps (in our examples, strain energy is calculated at every 2500 steps). Third, to speed up the computation further, the strain energy calculation does not extend over the whole system but only over a circular surface area of a given radius  $R$  around the point where the strain is to be evaluated, due to the rapid decay of this field as  $1/r^6$  (the radius  $R$  is taken to be 30 lattice grids).

### III. SIMULATION RESULTS

#### A. Dependence of island height on up-down ratio

Using the 3D QD self-assembly approach described above, we can now simulate the epitaxial growth process. The growth model is over  $100 \times 100$  grids with periodic boundary condition, and the model material is InAs/GaAs(001). Again, while there are two different species (In and As) in a compound InAs QD, we do not distinguish them in our KMC diffusion simulation,<sup>34</sup> and chemical species information is implied in the mismatch strain and elastic stiffnesses used in the strain energy calculation. We first study the effect of the up-down ratio on the island height. Shown in Fig. 3 are the island distributions for different up-down ratios. It is observed clearly from Fig. 3 that (1) the average island height increases with increasing up-down ratio  $\rho$  (for small up-down ratio, say,  $\rho \leq 5$ , basically only 2D growth mode can be observed); (2) the island size and shape are very sensitive to the up-down ratio  $\rho$  when it is less than 20; (3) the ratio  $P_{\text{up}}/P_{\text{down}}$  determines the 2D to 3D transition, instead of the absolute values of  $P_{\text{up}}$  and  $P_{\text{down}}$ . This ratio is directly proportional to the ratio of the ascending (desorption) and descending (adsorption) atoms on the surface,<sup>29,41</sup> and could be further related to the surface and bulk energy ratio in the system.<sup>12,18</sup>

To further understand the effect of the up-down ratio on the average island height, the data in Fig. 3 along with more simulated results for large up-down ratios are analyzed quantitatively. The relation between the average island height and

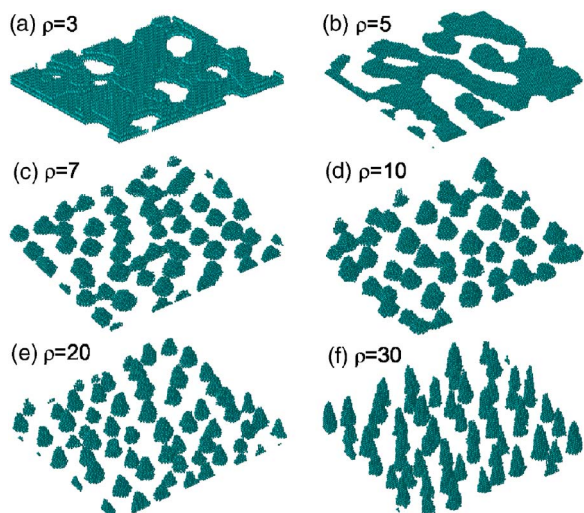


FIG. 3. (Color online) 3D island distributions for different up-down ratios  $\rho$  with total coverage  $c=1.6$  monolayers (ML). Fixed growth parameters are temperature  $T=700$  K, flux rate  $F=0.01$  ML/s, and interruption time  $t_i=200$  s [total simulation time=deposition time ( $t_d=160$  s) plus interruption time ( $t_i=200$  s)].

the up-down ratio is presented in Fig. 4, and, interestingly, it is similar to that in Ref. 23 based on a different simulation approach. Figure 4 also clearly demonstrates the following. (1) The average island height experiences sharp changes when the up-down ratio varies from 3 to around 20. In other words, the average island height in this range of up-down ratios is very sensitive to the up-down ratio, and that the islands become higher with increasing up-down ratio. (2) When  $\rho$  is larger than 20, the curve flattens to a horizontal line. This means that the average island height will mostly keep at a constant maximum value when the up-down ratio is large (say,  $\rho > 30$ ). (3) The inflection point approximately at  $\rho=13$  physically corresponds to the critical transition point from 2D cluster (flat pyramids) growth to 3D island (sharp domes) growth,<sup>9,11,12,18</sup> and this up-down ratio could be connected to the surface and bulk energy ratio.<sup>42</sup> Our critical value of  $\rho=13$  also agrees with previous calculations<sup>23</sup> showing flattened pyramids at  $\rho=6$  and sharp domes at  $\rho=15$ .

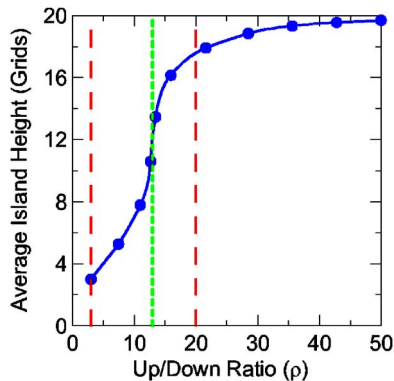


FIG. 4. (Color online) Average island height vs up-down ratio  $\rho$  (for  $\rho$  from 3 to 50). Fixed growth parameters are temperature  $T=700$  K, flux rate  $F=0.01$  ML/s, total coverage  $c=1.6$  ML, and interruption time  $t_i=200$  s.

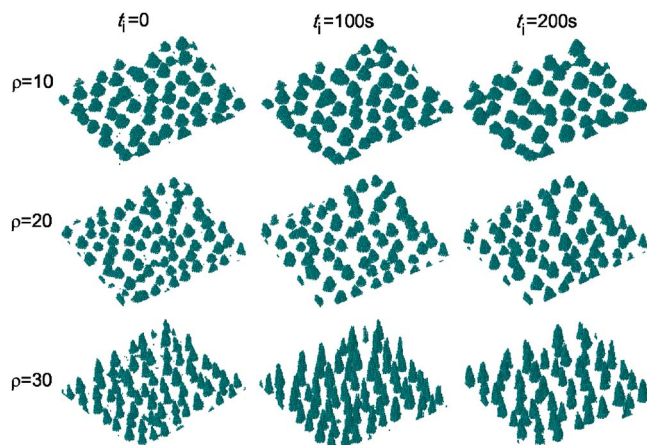


FIG. 5. (Color online) Island distributions for different interruption times ( $t_i=0$ , corresponding to deposition time  $t_d=160$  s,  $t_i=100$  s, and  $t_i=200$  s) and for different up-down ratios ( $\rho=10, 20$ , and  $30$ ). Fixed growth parameters are temperature  $T=700$  K, flux rate  $F=0.01$  ML/s, and total coverage  $c=1.6$  ML.

### B. Island size distributions

Island size equalization relies on the movement of atoms on the surface during epitaxial growth. It could start at the very beginning of the deposition process if a low flux rate is given.<sup>24,25</sup> Figure 5 demonstrates the island size dependence on growth times for three different up-down ratios ( $\rho=10, 20$ , and  $30$  in the first, second, and third rows) under a relatively low flux rate  $F=0.01$  ML/s. Island distributions immediately after the deposition (i.e., the interruption time  $t_i=0$ ) are shown in the first column, 100 s after the deposition ( $t_i=100$  s) in the second column, and 200 s after deposition ( $t_i=200$  s) in the third column (Fig. 5). It is observed from Fig. 5 that (1) island size equalization starts at the very beginning and continues with increasing interruption time; (2) for a fixed up-down ratio ( $\rho=10, 20$ , and  $30$ ), with increasing interruption time, small isolated islands tend to join onto the large ones in their proximity, and the island distribution becomes more and more ordered; (3) for fixed interruption time ( $t_i=0, 100$  s, and  $200$  s), an increasing up-down ratio, in general, increases the height of the islands (changes the shape of the islands), just as we have observed from Fig. 3. Since the up-down ratio is closely related to the surface and bulk energy ratio, this could provide experimentalists the opportunity to control and optimize the island shape and distribution.

While Fig. 5 illustrates the influence of the interruption time on the island size, Figs. 6 and 7 demonstrate further the effect of the deposition time on the island shape and size for fixed up-down ratio  $\rho=10$ . It is clearly observed from Fig. 6 that, again, island size equalization starts from the very beginning of the deposition process and it becomes large with increasing deposition ( $t_d=50, 100$ , and  $160$  s) and interruption ( $t_i=200$  s) time. Figure 6 furthermore demonstrates that, with increasing island size, the number of islands decreases (small islands join onto the neighboring large ones). The size change of the islands during growth can also be observed clearly from the same zoom-in island in Fig. 6 where both its height and lateral dimension are seen to increase dramati-

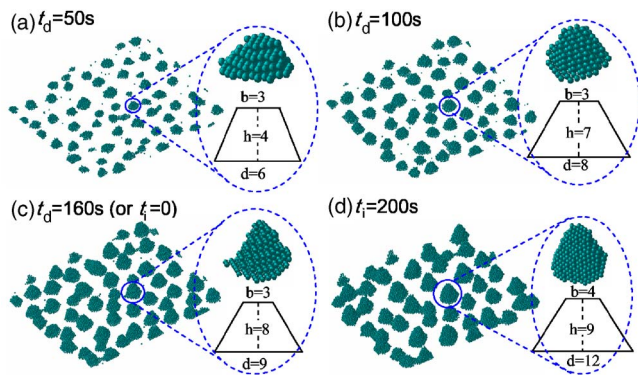


FIG. 6. (Color online) Island distributions during and after deposition. Deposition time (a)  $t_d=50$  s with 0.5 ML coverage, (b)  $t_d=100$  s with 1 ML coverage, (c)  $t_d=160$  s with 1.6 ML coverage (i.e., at the beginning of the interruption time), and (d) interruption time  $t_i=200$  s. Fixed growth parameters are temperature  $T=700$  K, flux rate  $F=0.01$  ML/s, total coverage  $c=1.6$  ML, and up-down ratio  $\rho=10$ . The zoom-in for the same island during the deposition and interruption time shows clearly the island size change (height  $h$  and lateral dimensions  $b$  and  $d$ ) during growth.

cally during growth. Shown in Fig. 7 is the histogram for the relationship between the island diameter (of the equivalent circle at the bottom of the island) and the corresponding number of islands, which again displays clearly the island size and number variation during growth.

Finally, Fig. 8 shows the effect of the flux rate ( $F=1$ , 0.1, and 0.01 ML/s) on the island distribution. For a low flux rate (e.g., at  $F=0.01$  ML/s), the deposited atoms have more time to move to the equilibrium position during the deposition process and to assemble together. Furthermore, a low flux

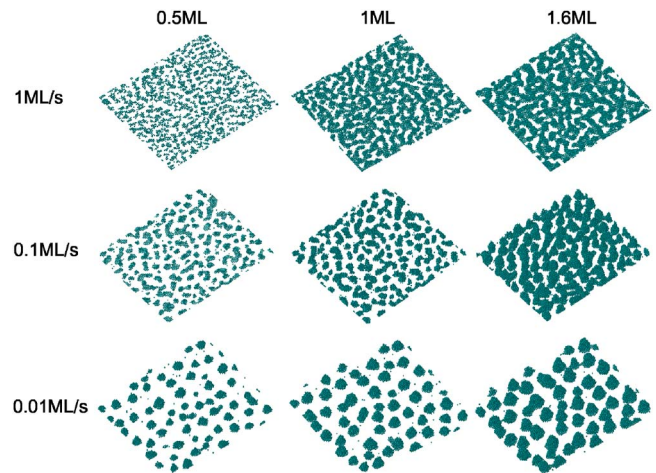


FIG. 8. (Color online) Island distributions for different deposition processes of 0.5, 1, and 1.6 ML with flux rates  $F=1$ , 0.1, and 0.01 ML/s. Fixed growth parameters are temperature  $T=700$  K, total coverage  $c=1.6$  ML, and up-down ratio  $\rho=10$ .

rate (say,  $F=0.01$  ML/s) usually corresponds to large and ordered islands. Therefore, besides the up-down ratio, the flux rate is also important in order to obtain an ordered and uniform-size QD island distribution. This is particularly true as a low flux rate is required for size equalization starting from the beginning of the deposition.

#### IV. CONCLUSION

In this paper, we propose a 3D QDs epitaxial growth model by enhancing our former  $(x,y)$ -plane growth model

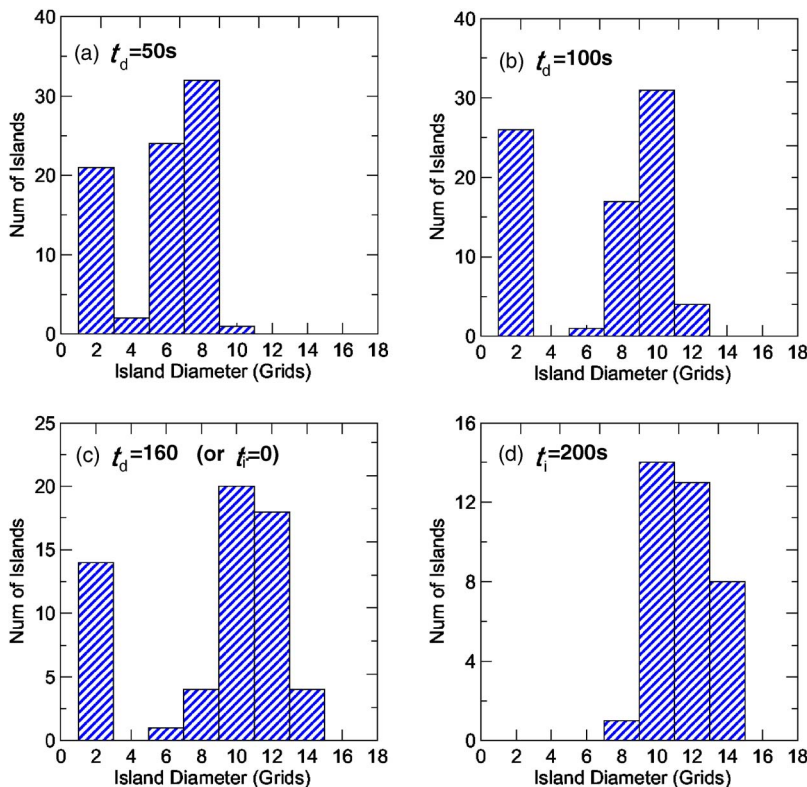


FIG. 7. (Color online) Average island diameter (of the bottom equivalent circle of the island) vs number of islands during and after deposition. Fixed growth parameters are temperature  $T=700$  K, flux rate  $F=0.01$  ML/s, total coverage  $c=1.6$  ML and up-down ratio  $\rho=10$ .

with a fast algorithm for long-range strain energy calculation and an up-down jump ratio for the diffusing atoms. Specifically, the balance between surface energy increase and bulk energy decrease in growth is demonstrated by introducing the up-down ratio. Further studied is the dependence of the island height and shape on the up-down ratio. Combining the up-down ratio and one of the growth parameters (i.e., flux rate), island equalization during and after deposition is demonstrated. The main conclusions from our 3D KMC model are as follows.

(1) The phenomena of self-assembly and shape transition of the islands (i.e., from flat pyramids to sharp domes) can be simulated by changing the up-down ratio.

(2) For other fixed growth parameters, island height and size greatly depend on the up-down ratio. For the examples used in this paper, the average island height increases with increasing up-down ratio and island size and shape are also very sensitive to the up-down ratio when it is less than 20.

Furthermore, we found that a critical value of the up-down ratio is around 13 where the QD morphology can change significantly from flat to sharp 3D islands.

(3) It is the up-down ratio, the ratio that characterizes the atom probability of jumping to the upper layer over that to the lower layer, that determines the QD sharp transition, instead of the absolute jump probability value.

(4) Island size equalization could start at the very beginning of deposition process if the flux rate is low. With increasing interruption time, an ordered island distribution with uniform size can be obtained.

#### ACKNOWLEDGMENT

We thank the reviewers for their helpful comments and suggestions. This work was supported by ARL under Grant No. W911NF-06-2-0038.

\*Email address: pan2@uakron.edu

- <sup>1</sup>V. Bressler-Hill, S. Varma, A. Lorke, B. Z. Nosho, P. M. Petroff, and W. H. Weinberg, *Phys. Rev. Lett.* **74**, 3209 (1995).
- <sup>2</sup>D. Bimberg, M. Grundmann, and N. N. Ledentsov, *Quantum Dot Heterostructures* (Wiley, Chichester, 1998).
- <sup>3</sup>J. Stangl, V. Holy, and G. Bauer, *Rev. Mod. Phys.* **76**, 725 (2004).
- <sup>4</sup>B. A. Joyce and D. D. Vvedensky, *Mater. Sci. Eng., R.*, **46**, 127 (2004).
- <sup>5</sup>P. Poloczec, G. Sek, J. Misiewicz, A. Loffler, J. P. Reithmaier, and A. Forchel, *J. Appl. Phys.* **100**, 013503 (2006).
- <sup>6</sup>O. P. Pcheljakov, V. A. Markov, A. I. Nikiforov, and L. V. Sokolov, *Thin Solid Films* **299**, 306 (1997).
- <sup>7</sup>V. A. Shchukin and D. Bimberg, *Rev. Mod. Phys.* **71**, 1125 (1999).
- <sup>8</sup>I. Daruka, J. Tersoff, and A. L. Barabasi, *Phys. Rev. Lett.* **82**, 2753 (1999).
- <sup>9</sup>G. Medeiros-Ribeiro, A. M. Bratkovski, T. I. Kamins, D. A. A. Ohlberg, and R. S. Williams, *Science* **279**, 353 (1998).
- <sup>10</sup>N. Moll, M. Scheffler, and E. Pehlke, *Phys. Rev. B* **58**, 4566 (1998).
- <sup>11</sup>F. M. Ross, J. Tersoff, and R. M. Tromp, *Phys. Rev. Lett.* **80**, 984 (1998).
- <sup>12</sup>F. M. Ross, R. M. Tromp, and M. C. Reuter, *Science* **286**, 1931 (1999).
- <sup>13</sup>F. Arciprete, E. Placidi, V. Sessi, M. Fanfoni, F. Patella, and A. Balzarotti, *Appl. Phys. Lett.* **89**, 041904 (2006).
- <sup>14</sup>Y. G. Musikhin, G. E. Cirlin, V. G. Dubrovskii, Y. B. Samsonenko, A. A. Tonkikh, N. A. Bert, and V. M. Ustinov, *Semiconductors* **39**, 820 (2005).
- <sup>15</sup>D. J. Shu, F. Liu, and X. G. Gong, *Phys. Rev. B* **64**, 245410 (2001); L. Huang, F. Liu, and X. G. Gong, *ibid.* **70**, 155320 (2004); L. Huang, F. Liu, G. H. Lu, and X. G. Gong, *Phys. Rev. Lett.* **96**, 016103 (2006); F. Liu, in *Handbook of Theoretical and Computational Nanotechnology* (American Scientific, Stevenson Ranch, CA, 2006), Vol. 4, pp. 577–625.
- <sup>16</sup>L. Y. Ma, L. Tang, Z. L. Guan, K. He, K. An, X. C. Ma, J. F. Jia, Q. K. Xue, Y. Han, S. Huang, and F. Liu, *Phys. Rev. Lett.* **97**, 266102 (2006).
- <sup>17</sup>E. Zoethout, O. Guerlue, H. J. W. Zandvliet, and B. Poelsema, *Surf. Sci.* **452**, 247 (2000).
- <sup>18</sup>C. W. Pao and D. J. Srolovitz, *Phys. Rev. Lett.* **96**, 186103 (2006).
- <sup>19</sup>C. W. Pao and D. J. Srolovitz, *J. Mech. Phys. Solids* **54**, 2527 (2006).
- <sup>20</sup>Y. Sun, T. Miyasato, and J. K. Wigmore, *J. Appl. Phys.* **87**, 8483 (2000).
- <sup>21</sup>R. Kern and P. Muller, *Surf. Sci.* **392**, 103 (1997).
- <sup>22</sup>S. A. Chaparro, Y. Zhang, J. Drucker, D. Chandrasekhar, and D. J. Smith, *J. Appl. Phys.* **87**, 2245 (2000).
- <sup>23</sup>D. V. Brunev, I. G. Neizvestny, N. L. Shwartz, and Z. S. Yanovitskaja, *Nanotechnology* **12**, 413 (2001).
- <sup>24</sup>E. Pan, R. Zhu, and P. W. Chung, *J. Nanoeng. Nanosyst.* **218**, 71 (2004).
- <sup>25</sup>E. Pan, R. Zhu, and P. W. Chung, *J. Appl. Phys.* **100**, 013527 (2006).
- <sup>26</sup>R. Kunert, Ph.D. thesis, Institut für Theoretische Physik, Technische Universität Berlin, 2006.
- <sup>27</sup>E. Pan, *J. Appl. Phys.* **91**, 6379 (2002).
- <sup>28</sup>E. Pan and B. Yang, *Appl. Math. Model.* **27**, 307 (2003); E. Pan and P. W. Chung (unpublished).
- <sup>29</sup>R. Lam and D. G. Vlachos, *Phys. Rev. B* **64**, 035401 (2001).
- <sup>30</sup>M. T. Lung, C. H. Lam, and L. M. Sander, *Phys. Rev. Lett.* **95**, 086102 (2005).
- <sup>31</sup>C. H. Lam, C. K. Lee, and L. M. Sander, *Phys. Rev. Lett.* **89**, 216102 (2002).
- <sup>32</sup>L. Nurminen, A. Kuronen, and K. Kaski, *Phys. Rev. B* **63**, 035407 (2001).
- <sup>33</sup>M. I. Larsson, *Phys. Rev. B* **64**, 115428 (2001).
- <sup>34</sup>M. Meixner, R. Kunert, and E. Schöll, *Phys. Rev. B* **67**, 195301 (2003). M. Meixner, Ph.D. thesis, Institut für Theoretische Physik, Technische Universität Berlin, 2002; M. Meixner, E. Schöll, V. A. Shchukin, and D. Bimberg, *Phys. Rev. Lett.* **87**, 236101 (2001).

- <sup>35</sup>F. Montalenti and A. F. Voter, Phys. Rev. B **64**, 081401(R) (2001).
- <sup>36</sup>A. Malachias, S. Kycia, G. Medeiros-Ribeiro, R. Magalhaes-Paniago, T. I. Kamins, and R. S. Williams, Phys. Rev. Lett. **91**, 176101 (2003); G. Medeiros-Ribeiro, A. Malachias, S. Kycia, R. Magalhaes-Paniago, T. I. Kamins, and R. S. Williams, Appl. Phys. A: Mater. Sci. Process. **80**, 1211 (2005).
- <sup>37</sup>I. G. Neizvestny, L. N. Safronov, N. L. Shwartz, Z. S. Yanovitskaja, and A. V. Zverev, in Proceedings of the Eighth International Symposium “Nanostructures: Physics and Technology,” St Petersburg, Russia, 2000 (unpublished).
- <sup>38</sup>A. B. Bortz, M. H. Kalos, and J. L. L. Lebowitz, J. Comput. Phys. **17**, 10 (1975).
- <sup>39</sup>C. S. Deo and D. J. Srolovitz, Phys. Rev. B **63**, 165411 (2001); C. S. Deo, D. J. Srolovitz, W. Cai, and V. V. Bulatov, *ibid.* **71**, 014106 (2005).
- <sup>40</sup>E. Pan and F. G. Yuan, Int. J. Solids Struct. **37**, 5329 (2000); E. Pan, Proc. R. Soc. London, Ser. A **458**, 181 (2002).
- <sup>41</sup>G. Russo and P. Smereka, J. Comput. Phys. **214**, 809 (2006).
- <sup>42</sup>P. Kratzer, Q. K. K. Liu, P. Acosta-Diaz, C. Manzano, G. Costantini, R. Songmuang, A. Rastelli, O. G. Schmidt, and K. Kern, Phys. Rev. B **73**, 205347 (2006).